Journal of Materials Processing Tech. 247 (2017) 121–133

Contents lists available at ScienceDirect

Journal of Materials Processing Tech.

journal homepage: www.elsevier.com/locate/jmatprotec

Laser welding of steel to aluminium: Thermal modelling and joint strength analysis

Sonia Meco[a,*], Luis Cozzolino[a], Supriyo Ganguly[a], Stewart Williams[a], Norman McPherson[b]

[a] Welding Engineering and Laser Processing Centre, Cranfield University, University Way, Building 46, Cranfield, Bedfordshire MK43 0AL, United Kingdom
[b] University of Strathclyde, 16 Richmond Street, Glasgow G1 1XQ, Scotland, United Kingdom

ARTICLE INFO

Keywords:
Laser welding
Finite element analysis
Intermetallic compounds
Steel
Aluminium

ABSTRACT

The integrity of steel-aluminium dissimilar alloy joints is dependent on the thermal cycle applied during the joining process. The thermal field has a direct influence on the growth of the intermetallic compounds (IMC), which result from the reaction between iron (Fe) and aluminium (Al), but it also determines the size of the bonding area of the joint. A finite element (FE) thermal model was developed to predict the transient thermal cycle at the Fe-Al interface for different levels of applied energy by changing the power density and interaction time. The time-temperature profiles were correlated to the weld geometry, IMC layer thickness and mechanical strength. The experimental results showed that having a small bonding area is equally detrimental to the mechanical strength of the joint as having a thick IMC layer. The FE model suggested that comparing to time, the temperature is more important in laser welding of steel to aluminium as this is the factor which most contributes to the growth of the IMC layer and the formation of the bonding area. However, it was not possible to identify a thermal field able to produce simultaneously a large bonding area and a thin IMC layer to optimize the joint strength.

1. Introduction

In automotive and maritime industries hybrid structures using different metals have been a research focus for a long time. The main driving force for this is the complementary properties of the metals and the development of design efficient structures. However, for many metallic combinations joining can be difficult due to dissimilarities in physical properties or poor chemical compatibility. In particular, when joining steel to aluminium the reaction between atoms of iron (Fe) and aluminium (Al) during the joining process form brittle intermetallic compounds (IMCs) (Bouche et al., 1998; Springer et al., 2011). The mechanical strength of the joint is limited by the presence of these IMCs and therefore the amount of these compounds should be minimised.

Studies have been carried out either aiming to understand the mechanism of formation and growth of the Fe-Al IMC layer or to maximise the mechanical strength of joints produced with different joining processes and then correlating the IMC layer thickness with the joint strength (Bouche et al., 1998; Shahverdi et al., 2002). The outcome of this research showed the composition and morphology of Fe-Al IMCs, the theoretical diffusion equations calibrated against experimental validation which determine the growth rate of these IMCs, and most important, the key parameters in the formation and growth of the IMCs, time and temperature.

All fusion joining processes occur in transient conditions and it is not possible to control temperature and time independently. The IMC layer thickness and the weld geometry (in particular weld width) are determined by the thermal cycle applied to the joint. Therefore, to control these two factors it is necessary to understand the thermal cycle and their dependency on it. FEA is a useful tool to estimate the thermal cycle under different welding conditions, i.e. different energy levels.

The main advantages of laser conduction welding compared to arc welding are (1) the control of the melt pool geometry and dimension by varying the laser metal interaction, flexibly which would be hard to achieve by an arc source e.g. GTAW; (2) minimal heat affected zone due to higher energy density of the laser process; (3) high cooling and solidification rates restricts diffusion an important aspect for such jointing; (4) laser energy can be applied in the most focused and directional manner which would allow more control on the heat input and thereby IMC formation. What is furthermore important is that with TIG it would not be possible to control the temperature gradient in a manner that only sufficient heat reaches near the interface to melt the aluminium alloy and wet the steel. Such control would not be possible

* Corresponding author.
E-mail addresses: s.a.martinsmeco@cranfield.ac.uk, aocem26@gmail.com (S. Meco), daniel.cozzolino@cranfield.ac.uk (L. Cozzolino), s.ganguly@cranfield.ac.uk (S. Ganguly), s.williams@cranfield.ac.uk (S. Williams), norman.mcpherson@strath.ac.uk (N. McPherson).

http://dx.doi.org/10.1016/j.jmatprotec.2017.04.002
Received 14 July 2016; Received in revised form 4 April 2017; Accepted 5 April 2017
Available online 10 April 2017

Table 1
Chemical composition of base metals.

Material	Elements (wt.%)												
	Al	Fe	C	Si	Mn	P + S	Ni	Ti	Cu	Mg	Zn	Cr	Other
XF350	0.047	Bal.	0.059	0.021	0.610	0.025	0.020	0.001	0.03	–	–	0.030	0.255
5083-H22	Bal.	0.400	–	0.400	0.500	–	–	0.150	0.100	2.600–3.600	0.200	0.300	–

by traditional non-consumable processes such as TIG or plasma.

In laser welding there are only a few research papers published where the IMC layer thickness is correlated with time and temperature. Fan et al. measured the thermal cycle at the interface between steel and aluminium and correlated the laser power with the peak temperature, cooling time and with the IMC layer thickness (Fan et al., 2011). However, the authors have not considered the two other important laser processing parameters, travel speed and laser beam diameter. The results showed that the IMC layer thickness was dependent on both peak temperature and cooling time. It is important to refer that in fusion joining processes as temperature and time are inter-dependent parameters, therefore when temperature increases, the time that the material is above a certain temperature also increases. FEA was used by Borrisutthekul et al. to predict the transient thermal cycle at the interface of the lap joints (Borrisutthekul et al., 2007). In this case the authors only assessed the influence of welding speed (or travel speed) and the material of the backing bars (heat sink) on the IMC layer growth. They showed that higher travel speeds and backing bars made of high thermal conductive materials minimise the IMC layer thickness. Once again, the authors have not considered the effect of laser power and laser beam diameter in the IMC layer growth. In equilibrium conditions, Wang et al. studied the formation of IMCs in Fe-Al alloys by heat treatment and also concluded that the IMC layer grows with both temperature and time (Wang et al., 1998). The authors also showed that time, as opposed to temperature, does not change the IMC composition.

In published work only IMC layer thickness has been correlated with mechanical strength of the joints whereas the dimension of the bonding between the steel and aluminium has been disregarded. One would expect the mechanical strength to follow a linear evolution with bonding area. However, the linear trend is not observed due to the continuous IMC layer formed at the joint interface. Also, Schubert et al. and Ozaki et al. estimated that an IMC layer thickness up to 10 μm would produce strong Fe-Al hybrid joints (Schubert et al., 1997; Ozaki and Kutsuna, 2009). However, if there is a positive effect in using very low energy in the joining process to suppress growth of the IMC layer, it is also true that this results in a small bonding area which reduces the joint strength. The temperature profile during the joining process determines both IMC layer thickness and bonding width. Therefore, it is important to characterise the evolution of these factors in terms of time and temperature so that the process can be optimised to achieve the best possible combination of mechanical strength and toughness. Previous research by Meco et al. showed that by increasing the amount of energy, by increasing power density, interaction time or laser beam area, both IMC layer thickness and bonding area were increased in laser welded joints (Meco et al., 2014). A larger bonding area contributes to a stronger joint but conversely, a thicker IMC layer is detrimental to the joint. It is therefore important to find a balance between these two parameters to obtain optimized joint strength. Mathieu et al. have discussed the importance of global geometry of fillet welds in laser brazing applied to steel to aluminium joints (Mathieu et al., 2007). The authors concluded that the geometry of the weld (concavity and wetting) plays an important role in the mechanical strength of the joint after observing samples with IMC layer thickness less than 10 μm but still showing poor mechanical properties.

The fundamental laser material interaction parameters, including power density or intensity (Eq. (1)), interaction time (Eq. (2)) and specific point energy (Eq. (3)) are used in this work. These parameters fully determine the way the material responds to the laser energy independent of the laser system in use (Suder and Williams, 2012) and determine the thermal cycle and cooling rate and thus, the weld geometry and microstructure changes (Williams and Suder, 2011). Therefore, the results obtained in this work can be applied or interpreted for any laser system.

- Power density, $MW.m^{-2}$ $$PD = P.\ A_{beam}^{-1} \quad (1)$$
- Interaction time, s $$t_i = D_{beam}.\ TS^{-1} \quad (2)$$
- Specific point energy, kJ $$E_{sp} = PD \times t_i \times A_{beam} \quad (3)$$

Power density is defined by the ratio of laser power and laser beam area projected on the substrate. In continuous laser mode, interaction time is defined as the ratio of beam diameter and travel speed. The specific point energy is the product of power density, interaction time and laser beam area and represents the total energy transferred to the work piece through the irradiated area.

The aim of this work is to understand how the IMCs and bond area affect the mechanical strength of the joints and how temperature and time affect these two parameters individually.

2. Materials and methodology

2.1. Materials

Plates of 2 mm low carbon steel (XF350) and 6 mm 5083-H22 aluminium alloy were used. The chemical composition and mechanical properties of the materials are detailed in Tables 1 and 2, respectively. The plates were 150 mm long and 138 mm wide, these dimensions were according to the standard for shear testing resistance seam welds (British Standard Instiurion, 2001).

All plates were cleaned before welding. The steel was ground and the aluminium was linished to remove any oxide layer from the surface. Afterwards all plates were degreased with acetone.

2.1.1. Laser welding

The joints were produced in a lap configuration with an overlap of 46 mm, with steel positioned on the top of aluminium (Fig. 1a). Laser welding in conduction mode was used because of the characteristic weld shape with low depth-to-width ratio. This welding mode is necessary for the joint configuration used in this work to avoid the mixing of the steel and aluminium in liquid state. This welding mode also avoids any vapourisation effects which leads to poor quality welds. In this manner, the heat produced when the laser beam irradiates on the steel surface is smoothly conducted through the thickness of the steel

Table 2
Mechanical properties of the base materials.

Material	Yield strength [MPa]	Ultimate tensile strength [MPa]	Total elongation at failure [%]
XF350	368	474	23 (at 80 mm of gauge length)
5083-H22	250	337	8 (at 50 mm of gauge length)

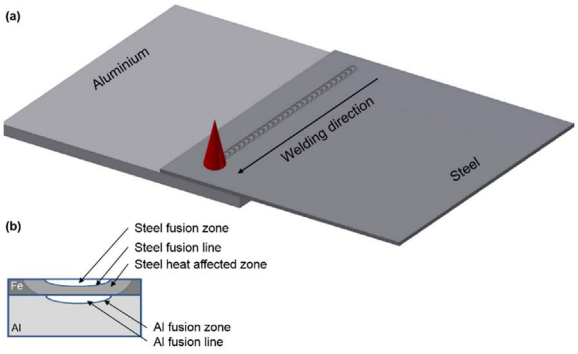

Fig. 1. Schematic representation of (a) the laser welding process and (b) the cross-sectional view of the weld seam. The cross-section shows two independent fusion profiles on the steel and aluminium plates which are important for this joining principle.

plate and induces local melting of the aluminium (Fig. 1b). The welding parameters must be controlled so that the temperature at the Fe-Al interface remains in the range between 570 °C ($T_{melting,Al}$) and 1500 °C ($T_{melting,steel}$). In this condition, the reaction between Fe and Al is better controlled than it would be if the joint was produced by melting both alloys (Ma et al., 2014). Thus, the formation of IMCs is minimised. The aspect ratio of the weld (penetration depth by weld width) gives an indication about the process mode. An aspect ratio smaller than 0.5 is characteristic of a weld produced in conduction mode (Quintino and Assuncao, 2013) (Fig. 1b).

Fig. 2 shows the clamping system used for laser welding.

The joints were produced with an IPG continuous wave fibre laser with 8000 W of maximum power and wavelength of 1.07 μm. The delivery system consisted of a fibre with 300 μm of diameter, a 125 mm collimating lens and a 500 mm focal length lens. The laser beam was characterized using a Primes GmbH focus monitor system and the D4σ method. The distance between the laser head and the substrate to have a laser beam diameter of 13 mm was determined based on the divergence of the laser beam and the focal position. It is known that a multimode laser beam in focus has a top hat intensity distribution but in out of focus condition, i.e. away from the focal plane position it has a Gaussian profile (Suder and Williams, 2012). Three different beam diameters were tested prior to this work, 10, 13 and 16 mm. It was found that with a 10 mm beam diameter the weld pool on the steel was narrower and deeper than that produced with larger beam diameters. Therefore, with a smaller laser beam the bonding area is smaller due to less melting of the aluminium and less wetting of the steel by the molten aluminium. To avoid this if the power density is increased then the temperature in the Fe-Al interface would be very large and would result faster diffusion and subsequently thicker intermetallic layer. The joints produced by 10 mm of beam diameter exhibited lower strength than those produced with larger beams e.g. 13 mm. However, when the laser beam was too large, it was more difficult to control the laser metal interaction to avoid full penetration on the steel plate and thus avoid

Table 3
System and fundamental laser material interaction parameters range.

System parameters			Fundamental laser material interaction parameters		
Beam diameter, D_{beam}[mm]	Power, P [kW]	Travel speed, TS [m min^{-1}]	Power density, PD [MW m^{-2}]	Interaction time, t_i[s]	Specific point energy, E_{sp}[kJ]
13.0	4.46–5.57	0.30–0.40	33.60–41.96	1.95–2.60	9.75–13.00

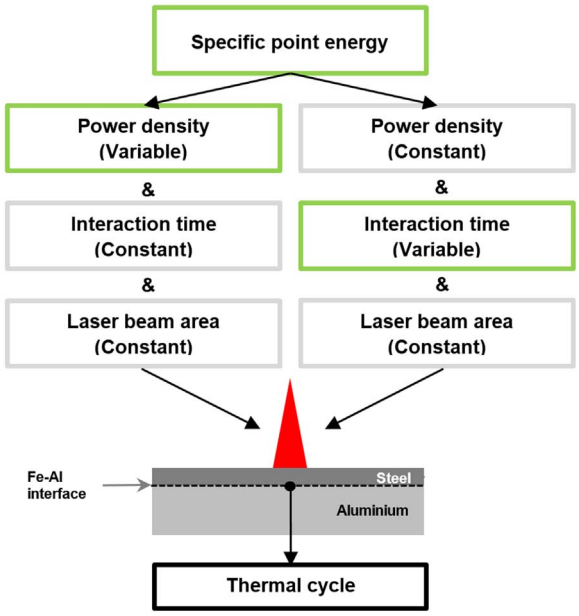

Fig. 3. Schematic representation of the methodology used in the welding experiments to assess the importance of the FLMIP on the thermal profile and consequently on the weld geometry and IMC formation.

the mixing of molten steel with aluminium. It was previously reported that the depth of a weld produced in conduction mode increases with the laser beam diameter, even though the power density decreases (Assuncao, 2012).

The range of laser system parameters and fundamental laser material interaction parameters (FLMIP) is given in Table 3. The working envelop is very narrow due to the joint configuration in use and the restriction that the steel near the joint interface must remain solid during the joining process. For this reason the welding parameters needed to be controlled to have only partial melting on the 2 mm thick steel plate. No shielding gas was used during the experimental work as the welding pool is formed at the interface and is normally protected

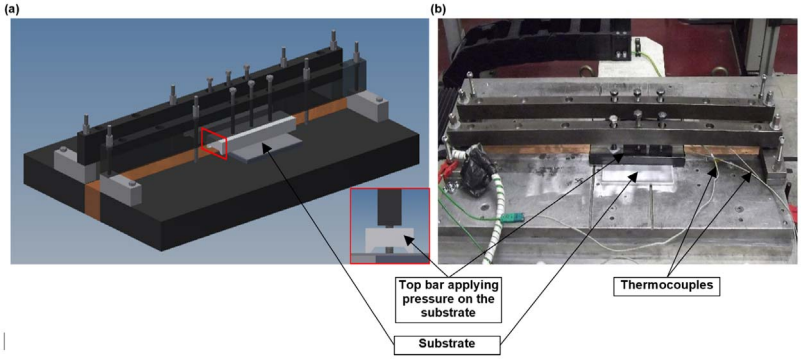

Fig. 2. (a) 3D CAD model and (b) picture of the clamping system used for laser welding.

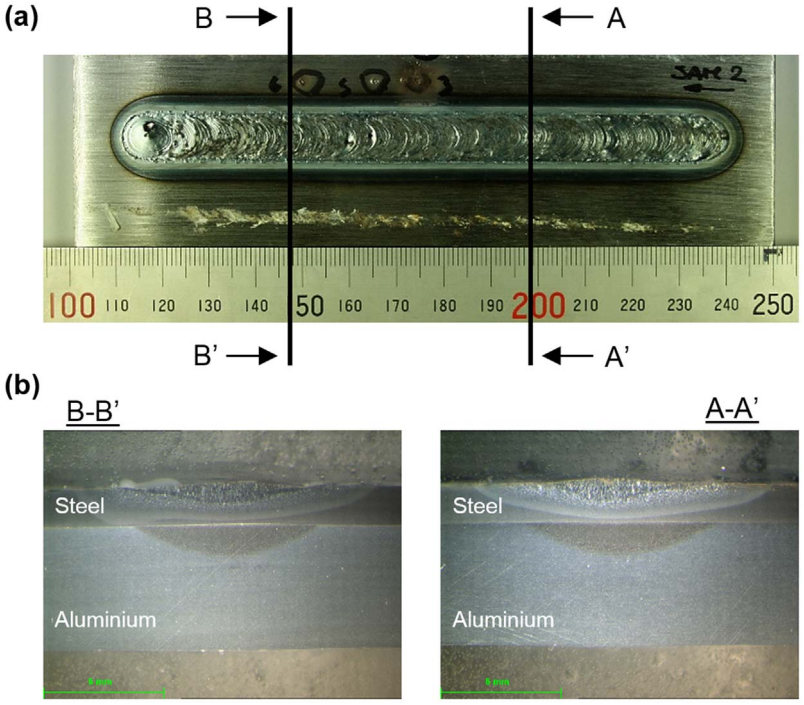

Fig. 4. Laser welding of steel to aluminium in steady state condition. (a) Top view of the welded joint showing a uniform weld seam and (b) cross-sections A–A' and B–B' showing similar weld geometries.

Table 4
Elements, nodes and element types used in the model.

Part	Abaqus element type	Number of elements	Number of nodes
Al plate	DCC3D8	438,084	479,960
Fe plate	DCC3D8	146,028	184,600
Fe insert	DCC3D8	41,884	53,960
Al insert	DCC3D8	125,652	140,296

from atmospheric gases.

The specific point energy was varied either by changing the power density or the interaction time (see Fig. 3). In turn, with laser beam diameter constant, the power density and interaction time varied with laser power and travel speed, respectively. The thermal cycle that results from the interaction of the laser with the material defines the bonding area created between the steel and the aluminium and the IMC layer thickness.

Similar methodology was previously used by Meco et al. where the individual effect of power density, interaction time, laser beam diameter and specific point energy on the IMC layer growth and bond

Table 5
Model parameters. *Convective heat transfer coefficients to mock the effect of the backing bar (conduction and thermal resistance).

Emissivity (Steel plate – Air)	0.8
Convective heat transfer coefficient (Steel plate – Air), W m^{-2} $°C^{-1}$	160
Convective heat transfer coefficient*(Aluminium plate – Aluminium backing bar), W m^{-2} $°C^{-1}$	7000
Convective heat transfer coefficient*(Aluminium plate – Copper backing bar), W m^{-2} $°C^{-1}$	3500
Thermal contact conductance between the tooling plates and the substrates, W m^{-2} $°C^{-1}$	
@ 0 m gap clearance	250,000
@ 0.01 m gap clearance	80,000
Thermal contact conductance at Fe-Al substrate interface in the weld region, W m^{-2} $°C^{-1}$	
@ 0 m gap clearance	300,000
@ 0.01 m gap clearance	80,000

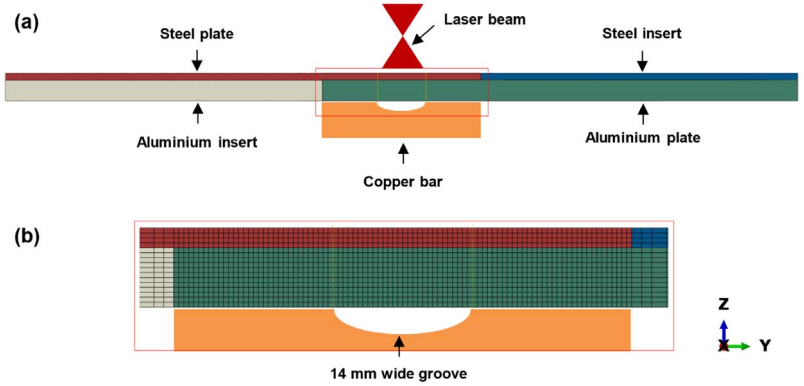

Fig. 5. Schematic representation of the transverse section of the weldment arrangement, including the steel and aluminium insert and copper backing-bar. (a) General view and (b) magnified view of the red rectangle shown in Fig. 5. (For interpretation of the references to colour in this figure legend, the reader is referred to the web version of this article.)

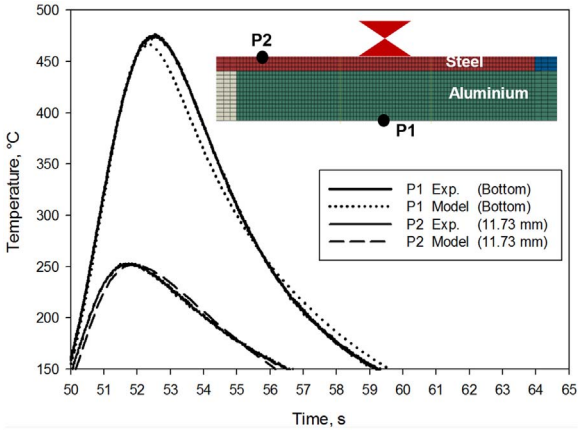

Fig. 6. Comparison between experimental and calculated thermal cycles at different distances from the weld seam (P = 5.0 kW, TS = 0.35 m min^{-1}, D_{beam} = 13 mm).

area was investigated (Meco et al., 2014).

2.1.2. Mechanical strength characterization

The mechanical strength of the joints was quantified by tensile-shear test. Straight sided specimens, 60 mm wide and 230 mm long, were tested according to EN ISO 14273:2001 standard (British Standard Instiurion, 2001). The tests were carried out at room temperature and a crosshead speed of 1 mm min^{-1}. The load was applied perpendicular to the weld seam and the deformation caused on the specimen was monitored by a laser extensometer with a gauge length of 50 mm.

2.1.3. Metallographic characterization

Cross-sections of the joints were produced for analysis of the weld geometry and the IMC layer thickness. The cross-sections were mounted in cold resin and then polished using the standard metallographic procedure. The aluminium and steel microstructures were etched using Keller's and 2% Nital etch solutions, respectively. The IMC layer thickness was measured according to the procedure described by (Meco et al., 2014). Macrographs were taken from the cross-sections

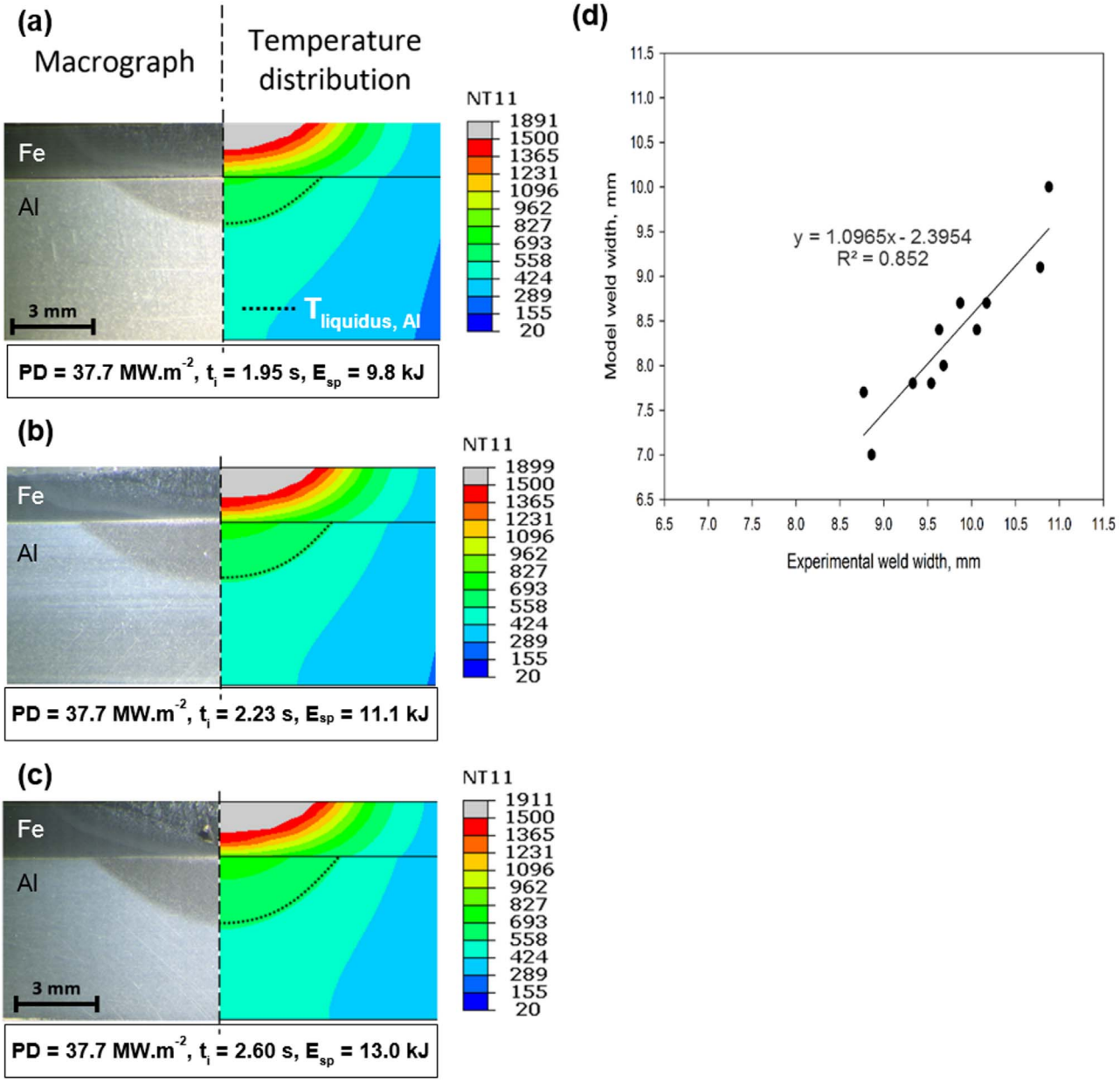

Fig. 7. Comparison between the experimental and the FEM results: (a-c) macrograph vs thermal profile and (d) experimental weld width vs weld width calculated by FEA.

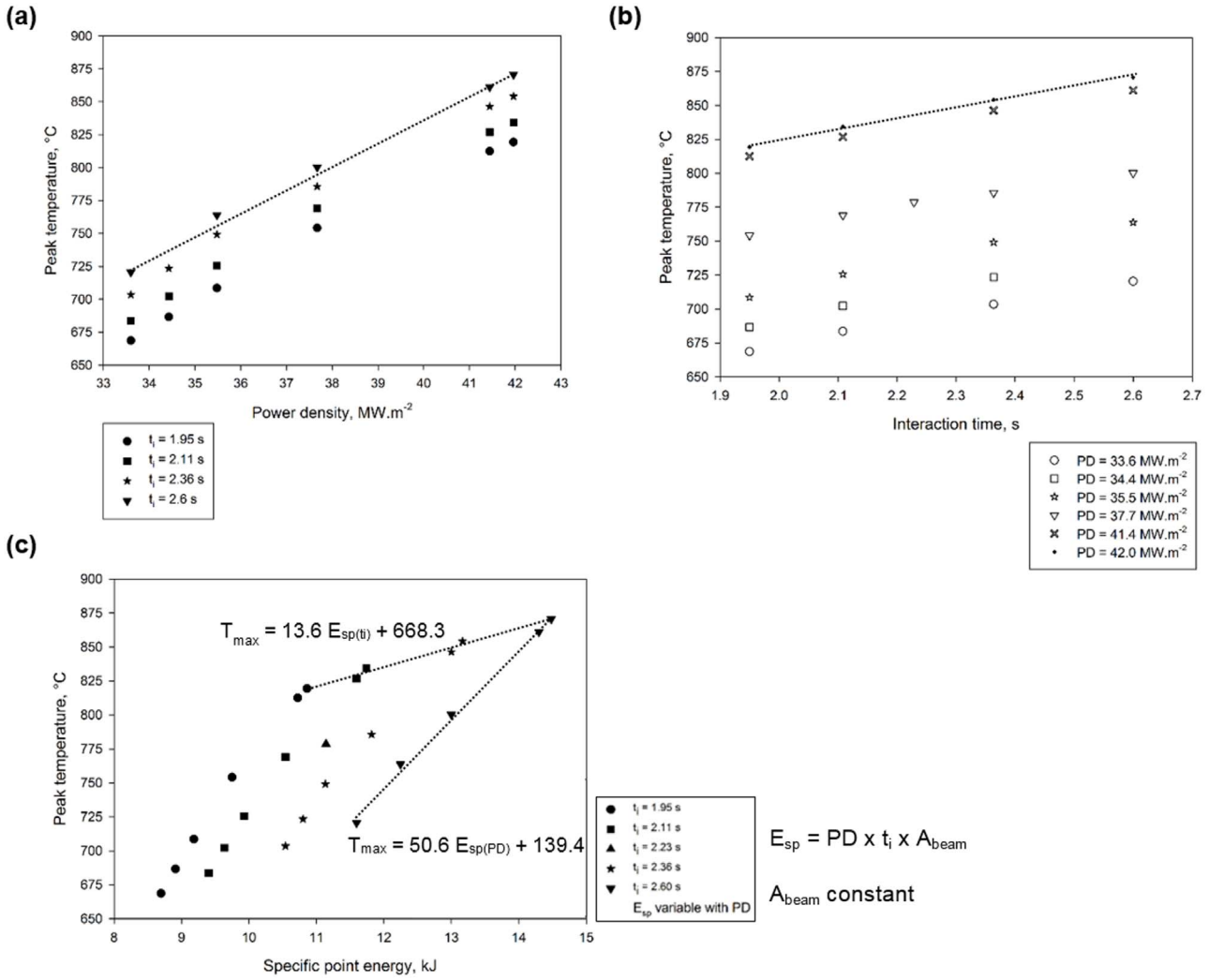

Fig. 8. Maximum temperature calculated by the FEA at the Fe-Al interface and at the centre of the weld for different levels of (a) power density, (b) interaction time and (c) specific point energy variable with power density (from 33.6 MW m^{-2} up to 42.0 MW m^{-2}).

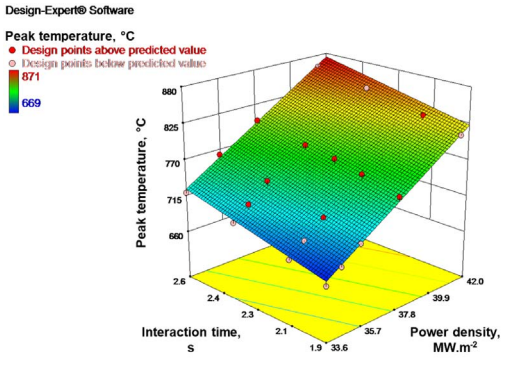

DOE equation with coded factors:

$$T_{max} = 775.24 + 73.87\,PD + 25.42\,t_i \quad (4)$$

Fig. 9. Graphical representation of peak temperature as a function of interaction time and power density.

where the fusion zones of the steel and aluminium were visible. Depth of penetration and weld width were measured using the digital imaging software AxioVision (Ltd., 2009).

2.1.4. Finite Element thermal model

FE models were developed to simulate the heat distribution produced by the laser welding process on the Fe-Al lap joints. The thermal cycles were calculated for the welding conditions indicated in Table 3. The aluminium 5083 and mild steel thermal properties were according to Kim et al. (2010) and Cozzolino (2013), respectively. These models were steady state heat transfer analyses, therefore the length of the modelled plates was assumed infinitely long to capture the entire heat cycle. At the point where the samples were taken the process was already in steady state condition because the weld seam was uniform and the weld profiles at the cross-sections A and B were similar, as shown in Fig. 4.

The type and number of elements and nodes is shown in Table 4.

The aluminium and mild steel plates were overlapped by 46 mm with the mild steel above the aluminium, as shown in Fig. 5. The additional tooling plates, also known as insert plates, used to ensure a flat surface for clamping were simulated to include the thermal losses in those components. The aluminium and steel tooling plates were 6 mm and 2 mm thick, respectively. The heat source used in the numerical model had a Gaussian intensity distribution and 13 mm of diameter to simulate the defocused laser beam used in the welding process.

In this model, the thermal losses into the surroundings were taken into account by applying constant convection and radiation from the outer surfaces (see values in Table 5). In the experiments, the plates were placed on a metallic backing support during welding. This backing

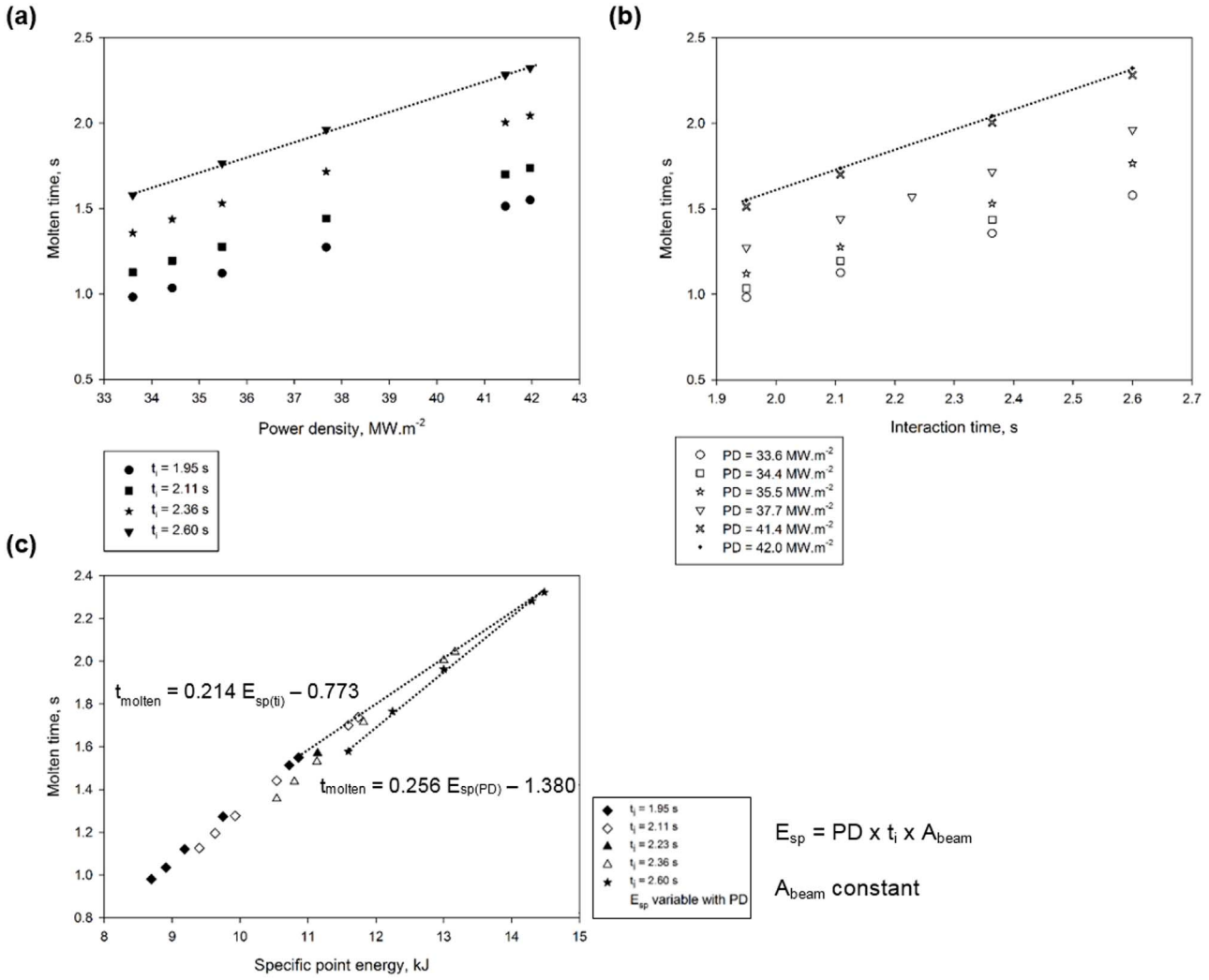

Fig. 10. Molten time calculated by the FEA at the Fe-Al interface and at the centre of the weld for different levels of (a) power density, (b) interaction time and (c) specific point energy variable with power density (from 33.6 MW m^{-2} up to 42.0 MW m^{-2}).

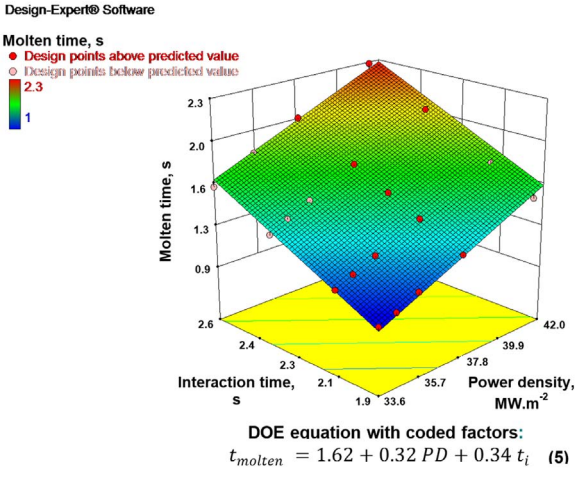

Fig. 11. Graphical representation of molten time (considering temperature at Fe-Al interface higher than 570 °C corresponding to aluminium in liquid state) as a function of interaction time and power density.

support was composed of an aluminium plate and a copper backing-bar positioned under the weld. The copper backing-bar had a square section with 46 mm in each side and a groove of 14 mm wide in the middle of the contact surface with the aluminium plate, as shown in Fig. 5. In the welding thermal models the backing bar can be modelled by two approaches: as a solid body with temperature dependent thermal resistance between the weld and the backing bar (Shi et al., 2003a, 2003b; Simar et al., 2007, 2006; Wang, 2011; Wang et al., 2013) or by modelling its heat sink effect, applying a temperature dependent convective heat sink in the expect contact area (Colegrove et al., 2009; Ding et al., 2011; Khandkar et al., 2003; Preston, 2000; Sun et al., 2009). The latter has the advantage of faster computational time. However, to obtain the correct parameters can be time consuming. The thermal losses into the backing support were modelled by applying forced convection with different convection coefficients. The top bars of the clamping system were insulated with a fibreglass insulation strip to make the heat loss from the top surface of the material negligible.

The thermal contact conductance between the tooling plates and the substrates was taken into account, as well as in the welding region. To simplify the model the thermal conductance was considered constant even though in the weld region it should be time dependent. The thermal conductance should increase when the aluminium becomes liquid and decrease when the IMC layer grows as this has a very low conductivity. These parameters were determined by iterative recalculation of the model and comparison of the thermal profiles with the experimental results (cooling rates to determine the thermal losses and the temperature rise to determine the absorbed energy). The pressure of the clamps applied onto the plates during the experiments was consistent in all the samples by using a torque wrench to tighten the

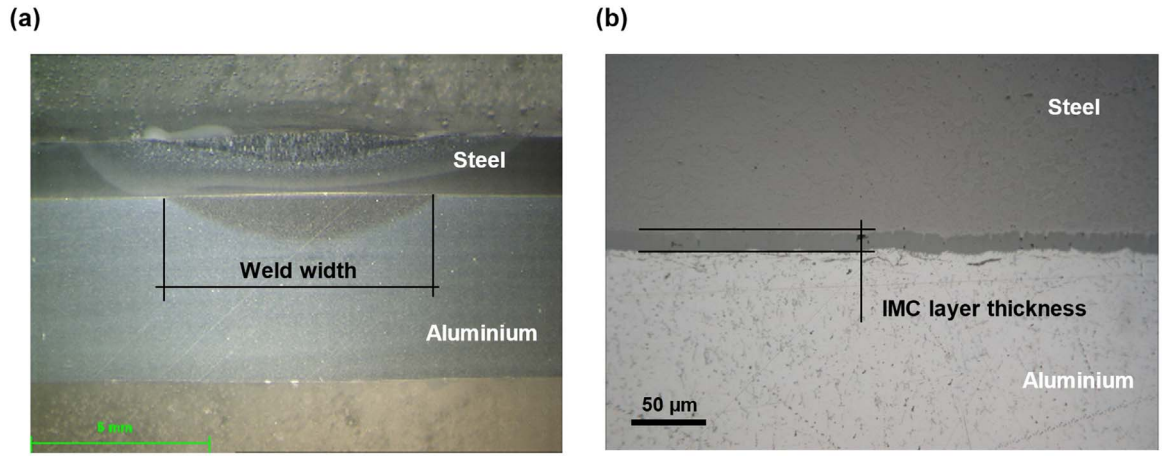

Fig. 12. Cross-sectional view of the laser welded Fe-Al joint: (a) macrograph and (b) micrograph.

bolts. Therefore, the thermal conductance was considered pressure independent. The pressure applied on the substrate is important to create a practically continuous jointing without any perceptible gap between the plates because the material surrounding the melt pool remains solid. Visual inspection is the easiest method to determine if the contact between the plates was lost during the welding process. If the heat resultant from the interaction of the laser with the steel is not uniformly transferred to the lower plate, the weld seam will not be uniform and in some cases will result in full penetration on the steel plate without any effect on the aluminium plate.

For calibration of the model several experiments were carried out with different interaction time and power density values. K-type thermocouples were attached to the surface of the specimens at different positions to measure the thermal cycle during welding.

3. Results and discussion

3.1. Process modelling and experimental validation

The thermal profiles calculated by the FEM at different positions were in good agreement with the experimentally measured values (see Fig. 6).

At two different positions on the sample, the peak temperature, heating and cooling phases from the model match the experimental data. The minimum temperature in this graph is 150 °C because from the relative importance below this value, diffusion of the atoms would be effectively slowed down to have any significant impact on the IMC layer composition and thickness. The heating phase and peak temperature in the model are related to the characteristics of the heat source, whereas the cooling phase is associated to the cooling conditions specified in the model. The cooling conditions need to take into account the material properties, contact between the steel and aluminium plates and the plates and the clamping system. The formation and growth of IMC layer may also play a role in the cooling of the material because during the joining process this layer grows and the heat conduction between both plates may change.

The aluminium weld width which defines the bonding area was also calculated by the model. For this, the area enclosed by the isotherm represented on the aluminium plate with temperature higher than the aluminium melting point was considered (see Fig. 7a–c). These figures show how the model compare to the experimental data. The isotherm line indicated on the picture from the model represents the liquidus temperature of the aluminium. The fusion zones of the three welds produced using different interaction times and constant power density are very similar to the ones represented by the model. Fig. 7d shows how the weld width estimated by the model compares to the experimental data. The experimental weld width showed a continuous and predictable difference with the modelled data. In the model the weld depth was matched with the experimental data as this is important to predict the temperature in the interface and at the bottom of the plate. The weld width in the model showed a lower value as compared to the experimental weld width. Additionally it showed a predictable difference which means as the welding process begins there is a change in contact at the interface which resulted in more heat conducted in the width direction as compared to the depth. The predictability in the difference is owing to very similar level of distortion which happens dynamically with the heat of welding when the process starts. Therefore, the graph shows the predictable difference which is from an inherent change in the experimental set up from the developed model during the process.

3.2. Power density and interaction time vs time and temperature

The peak temperature and molten time (time corresponding to the temperature at Fe-Al interface higher than 570 °C, which is the aluminium melting temperature) calculated by FEA were analysed separately for different levels of power density and interaction time. According to graphs in Fig. 8a and b, both interaction time and power density have direct influence on the maximum temperature of the thermal cycle. Fig. 8a shows the evolution of the peak temperature as a function of power density for different levels of interaction time. On the other hand, Fig. 8b shows the evolution of the peak temperature as a function of interaction time for different levels of power density. Compared to the interaction time, the power density induces a larger variation of the peak temperature. The slope of the trend lines in the graphs give an indication about the influence of each parameter on the peak temperature. In Fig. 8a the trend line is steeper than that in Fig. 8b. The analysis of the results in terms of specific point energy permits to understand the effect of power density and interaction time on the thermal cycle independent of the experimental range tested for each parameter. For this reason, the results were also presented as a function of process energy. In Fig. 8c the specific point energy is variable with power density and the interaction time is constant for each series of the graph. One may observe that within a given range of energy, the peak temperature has a larger variation when the power density varies than when interaction time varies. Considering the equations of the trend lines, the maximum temperature increases nearly 50 °C/kJ with power density and only 13 °C/kJ with interaction time.

The Design Expert software was used to create the surface plot represented in Fig. 9. The 3D graph has a linear regression of power density and interaction time as a function of peak temperature. The red dots correspond to the FEA model run points. Eq. (4) was obtained from the Design Expert software with coded factors to describe the trend of peak temperature in function of power density and interaction time

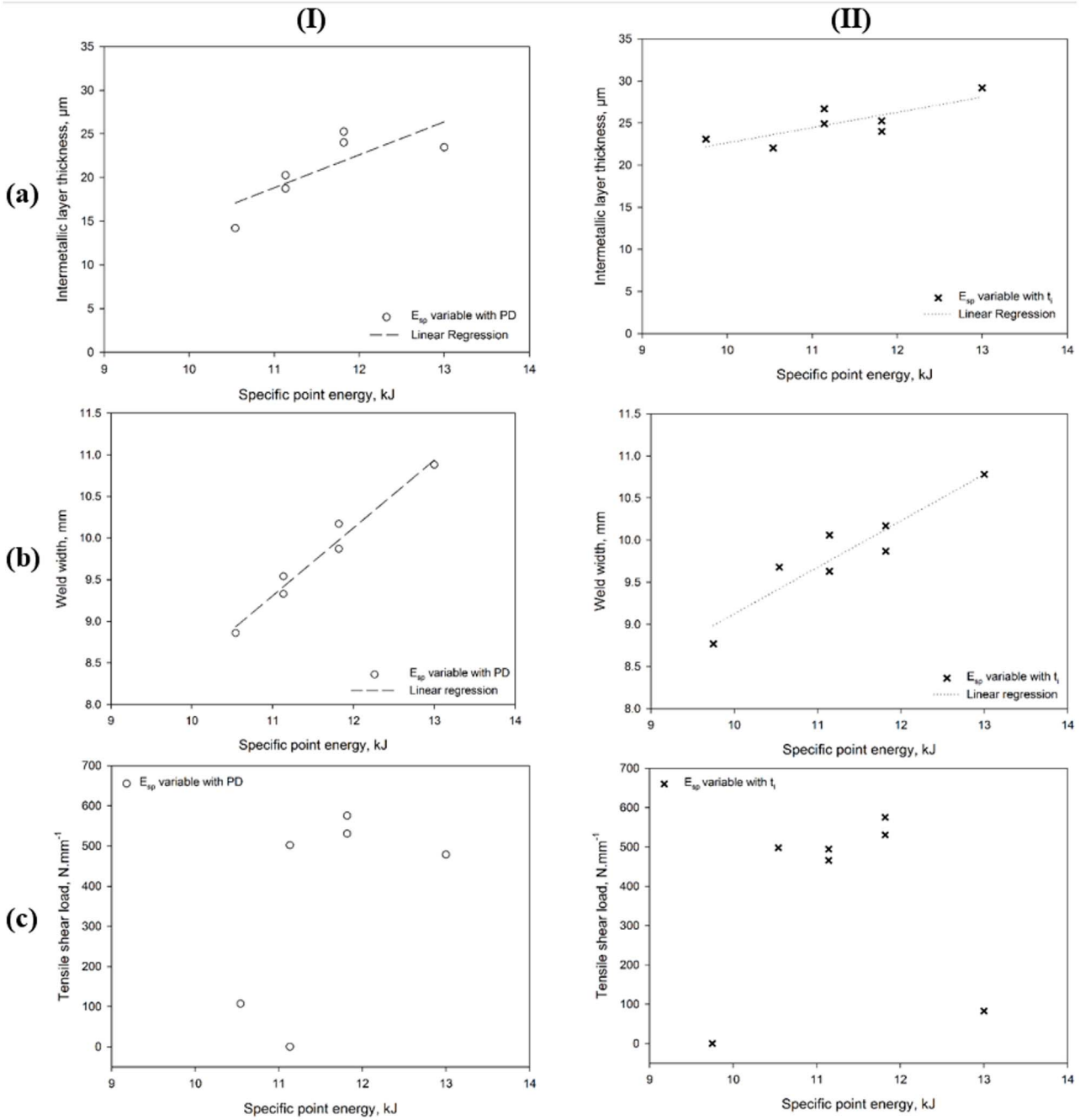

Fig. 13. Graphical representation of (a) IMC layer thickness, (b) weld width and (c) tensile shear strength as a function of specific point energy variable with (I) power density and (II) interaction time.

over the range of the experiments. The coded factors give an indication about the relative weight of each individual parameter on the peak temperature and the factors are independent on the magnitude of each parameter. In this case, power density has about three times more influence on the peak temperature than interaction time.

A similar approach was used to correlate the fundamental laser material interaction parameters with the molten time. The graphs in Fig. 10a and b show that a longer melting time results from either higher power density or longer interaction time. Opposed to the peak temperature, power density and interaction time have a similar effect on the molten time. The slope of the trend lines in Fig. 10a and b is similar. In terms of process energy, Fig. 10c shows that the time in molten state is directly proportional to specific point energy for any value of the power density or interaction time. Within a range of energy, the molten time increases 0.21 s/kJ with power density and 0.25 s/kJ with interaction time.

The surface plot represented in Fig. 11 is a linear regression of power density and interaction time as a function of molten time. The red dots correspond to the FEA model run points.

The coded factors in Eq. (5) for power density and interaction time are similar, 0.32 and 0.34 respectively. Once again this confirms that these two parameters have identical effect on the molten time. The effect of interaction time on molten time is clear, a longer interaction time allows the material to be in liquid state for a longer period of time. On the other hand, the effect of the power density is associated to the inter-dependency of temperature and time. This means that for a higher peak temperature there is a longer time in which the metal is above its melting temperature. As shown in Fig. 8, the peak temperature is highly dependent of power density, therefore a longer molten time is expected when power density increases.

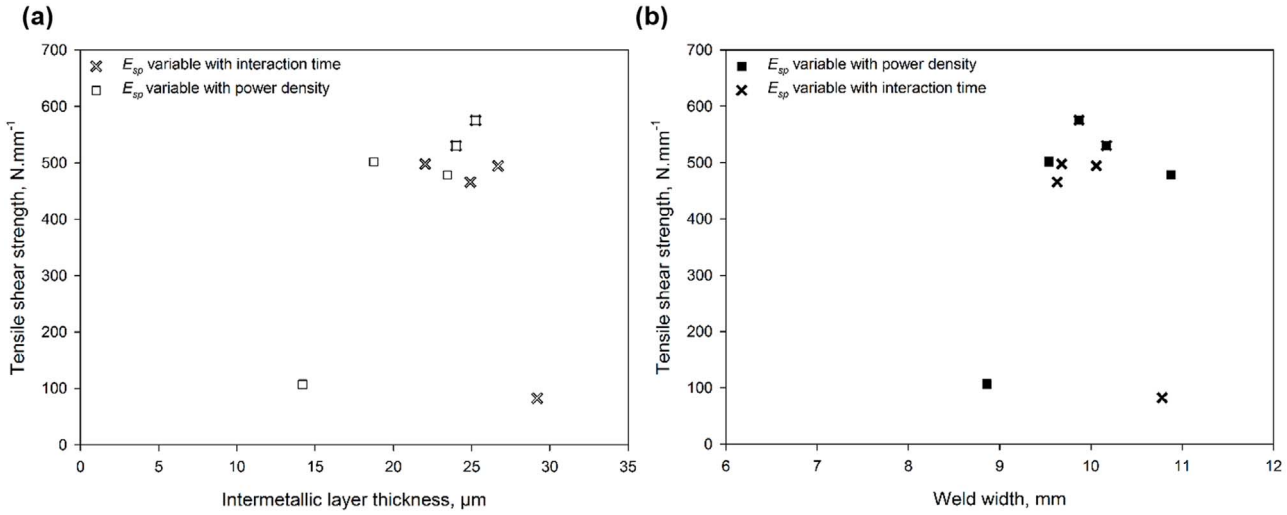

Fig. 14. Correlation between maximum tensile-shear strength and (a) IMC layer thickness and (b) weld width.

3.3. IMC layer thickness and weld width vs Joint strength

The cross-section of a laser welded joint is shown in Fig. 12a. The geometry of the fusion zone on the steel plate is characteristic of the welds in conduction mode. The macrograph also shows that the depth of penetration on the steel plate was less than half thickness (about 1 mm) and for this reason during joining there was no mixing of molten aluminium with molten steel. The IMC layer resultant from the reaction between atoms of Fe and Al is located between the steel and the aluminium plates, as shown in Fig. 12b. The bonding area between steel and aluminium is given by the width of the aluminium fusion zone, as indicated in Fig. 12a. The length of the weld was not considered because it was equal in all samples.

It is known that the thermal field resultant from the interaction of the laser with the material defines the dimension of the weld width and the IMC layer and the integrity of the joints is dependent on these two factors. However, when the thermal field is not known, the only way to correlate the welding process with the characteristics of the joints is by the process parameters. The graphs in Fig. 13a and b show how the IMC layer thickness and the weld width evolved with specific point energy, within the range of the experiments with either power density (I) or interaction time (II). As the energy of the process increases either by power density or interaction time, the IMC layer becomes thicker and the fusion zone of the aluminium becomes wider. This explains the non-linear behaviour of the mechanical strength of the joints with the specific point energy, which is represented in Fig. 13c. The joints have minimum strength when the process energy is either minimum or maximum. Fig. 14a and b show how the mechanical strength of the Fe-Al welded joints varies with IMC layer thickness and weld width formed during different welding conditions, respectively. Both graphs have similar trend, the mechanical strength is maximum only when the weld width and IMC layer have intermediate values. The thermal field during the welding process with high levels of energy induced the growth of the weld width and the IMC layer thickness simultaneously and these two parameters have opposite effects on the mechanical strength of the joints. When the weld width is large the IMC layer is very thick but when the IMC layer is thin the bonding area is very small. Therefore, only for intermediate values it is possible to a relative high strength. One would expect the mechanical strength of the joint to have a linear dependence with bonding area, however, in dissimilar metal joining an additional parameter must be taken into account, the IMC layer formed at the joint interface.

3.4. IMC layer thickness and weld width vs temperature and time

The results from the thermal model explain why the weld width and IMC layer thickness vary with specific point energy. It is clearly seen in Fig. 15c and d that the thermal field within the experimental range is linearly proportional to the specific point energy. The maximum weld width and IMC layer thickness formed on samples welded with high level of energy (indicated in Fig. 15a and b) are due to the maximum peak temperature and the molten time. At the joint interface and within the experimental range with energy varying with power density, the temperature of the molten aluminium ranged between 700 and 850 °C. When the energy varied with interaction time, the range of temperature was from 750 up to 800 °C. In terms of time, the model estimated that independent of the way the energy was varied the aluminium remained in liquid state between 1.3 and 2.0 s.

The effect of temperature and time on the IMC layer thickness and weld width was analysed separately in Figs. 16 and 17, respectively. The results suggest that the IMC layer thickness is more dependent on peak temperature than that on time. As the temperature increases with the process energy, the IMC layer becomes thicker. This result is in agreement with the results published by other authors, in which the experiments were either in equilibrium conditions (Wang et al., 1998) or transient conditions (Fan et al., 2011). On the other hand, the molten time seems to not have a direct correlation with the IMC layer thickness. For instance, when the molten time is about 1.4 s, the IMC layer can be either 15 or 22 µm. Even though the molten time is similar, the peak temperature of these two points is different due to the inter-dependency of temperature and time. This results suggest that within the experimental range, the IMC growth is more influenced by temperature than by the time.

Fig. 17 shows how the weld width calculated by the FEA thermal model varies with the thermal profile during laser welding.

Considering the equation produced by the DOE model, it is possible to infer that the peak temperature is the parameter which most contributes to the formation of a larger bonding area. The peak temperature is about three times more important than molten time (see Eq. (6)). The temperature field given by the model for different levels of power density and interaction time are shown in Fig. 18. For a fixed energy input, 11 kJ for instance, the aluminium fusion zone is wider when higher power density and shorter interaction time are used to produce the joint.

This result corroborates what has been suggested in a previous work where it was referred that the weld width increases with power density due to the peak temperature (Meco et al., 2014). The profile of the laser beam may be a reason for the growth of the weld width with power

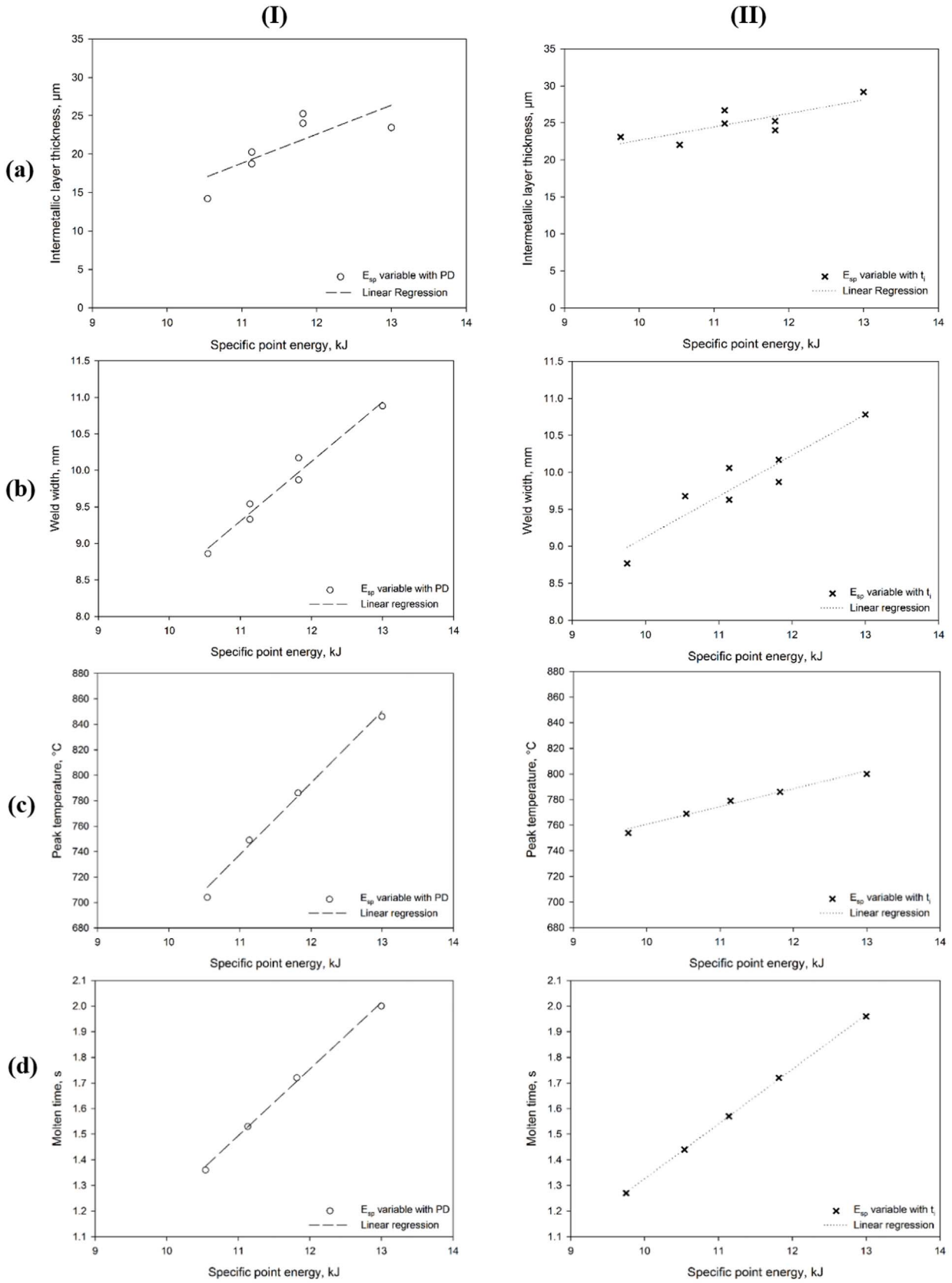

Fig. 15. Graphical representation of (a) IMC layer thickness, (b) weld width, (c) peak temperature and (d) molten time as a function of specific point energy variable with (I) power density and (II) interaction time.

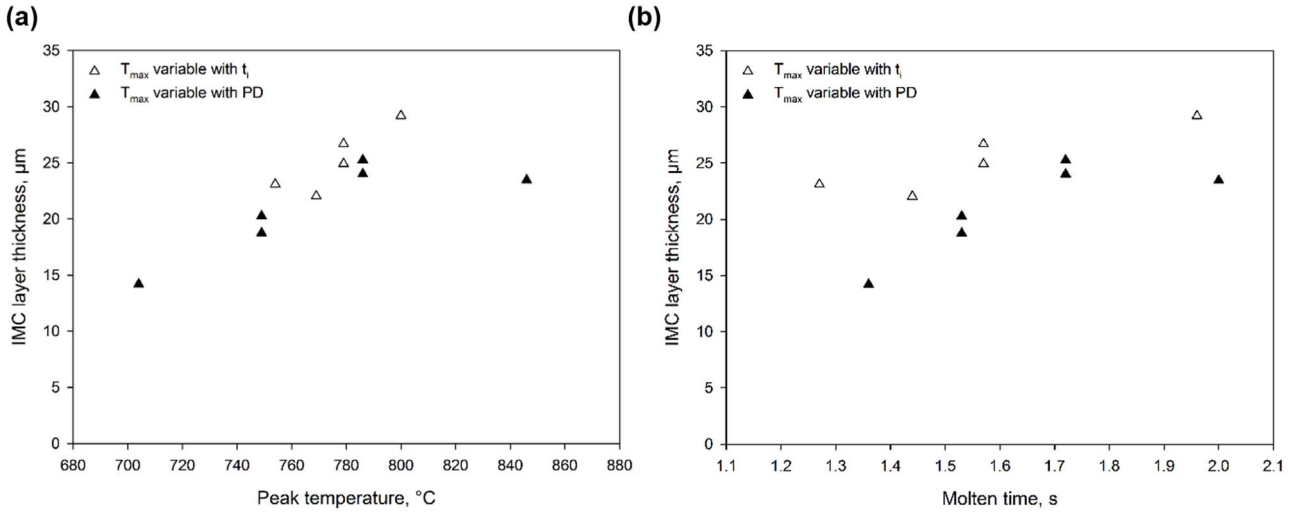

Fig. 16. Correlation between IMC layer thickness and (a) peak temperature and (b) molten time.

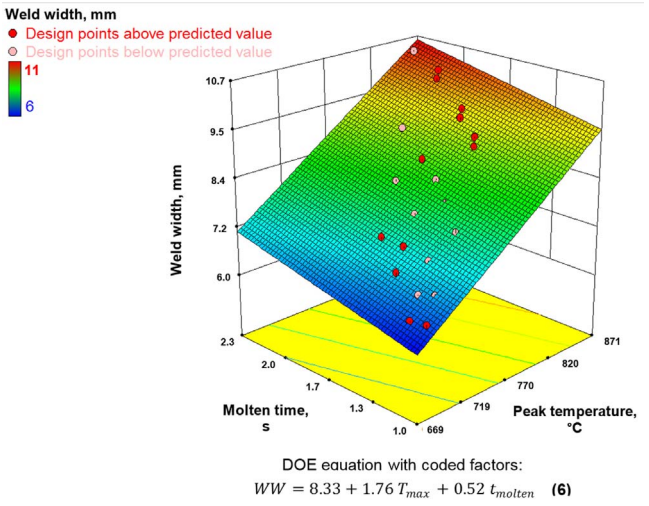

Fig. 17. Surface plot of weld width as a function of peak temperature and molten time.

density. If the laser beam has a Gaussian profile, as the power density increases the effective size of the laser beam also increases. This effect has also been observed in laser cutting where it was found that the kerf width changed when increasing the laser power for a constant nominal beam diameter. The authors attributed the changes in kerf width to the non-perfect top hat power distribution. As the power density increases, the effective beam diameter increases due to the edges of the beam profile not being perpendicular. Therefore, by increasing the power, the diameter of the beam which exceeds the energy density threshold for melting of the material also increases. Then, this results in increasing the width of the weld. With a perfect top hat profile this effect would not be seen.

The results of this work suggests that it is not possible to further improve the mechanical strength of the Fe-Al joints by solely controlling the energy of the process. The IMC layer and the bonding area are the key factors for the integrity of the Fe-Al joints and both evolve in a similar manner with the thermal field, i.e. temperature and time. To improve the mechanical strength of the joints by increasing the bonding area, it would be beneficial to increase the power density because this

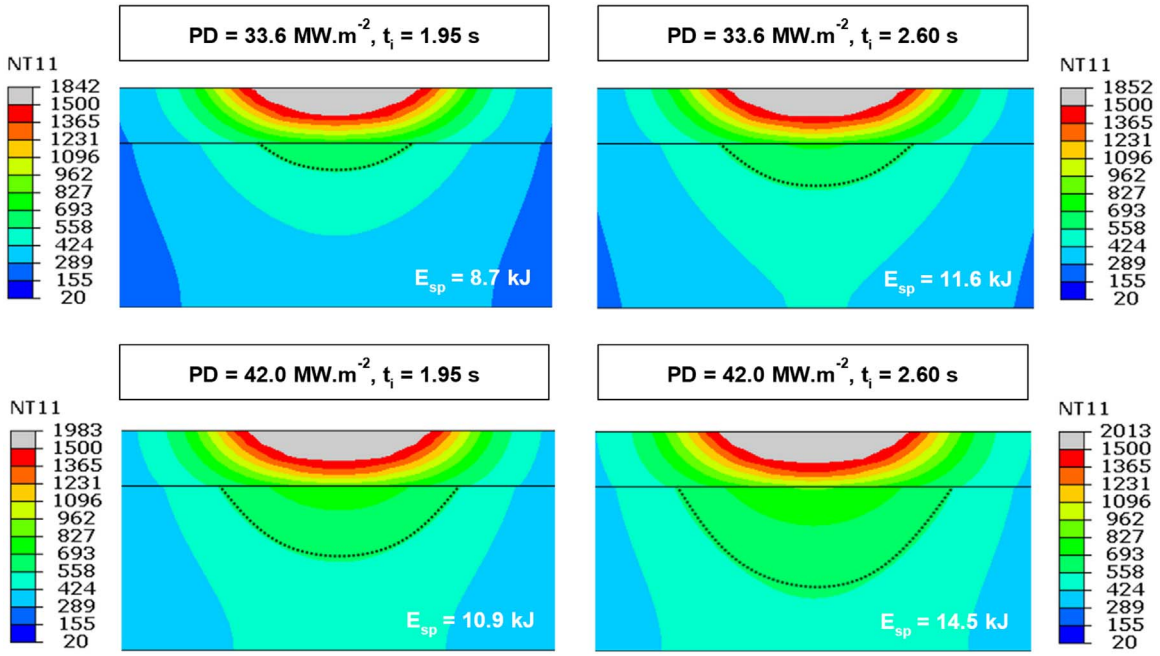

Fig. 18. Temperature distribution on the plane perpendicular to the weld seam for different values of power density and interaction time.

creates a larger weld. However, the power density is the parameter which most controls the temperature and since the IMC layer seems to be more sensitive to temperature than that to time under this welding condition the IMC growth would be also enhanced. An alternative solution to increase the bonding area and avoiding the negative effect of the IMCs could be by producing parallel weld seams.

4. Conclusions

It is known that IMC layer thickness and bonding area play an important role on the mechanical strength of dissimilar metal joints of steel to aluminium. In this work a FE model of the laser process was developed to predict the thermal cycle at the interface between the steel and aluminium plates using different laser parameters. The influence of the thermal cycle was correlated to the bonding area (via weld width) and to the IMC layer thickness and in turn, to the mechanical strength of the joints. Conclusions from this work are as follows:

- Power density is the factor with major significance in the variance of peak temperature, about three times more than interaction time;
- In terms of time in molten state (time correspondent to temperature higher than the aluminium melting point), power density and interaction time have similar contribution;
- Within the range of the experiments, the peak temperature and molten time are directly proportional to specific point energy (either via power density or interaction time);
- The strength of the joints increase with bonding area (defined by the width of the aluminium weld) and decreases with the IMC layer thickness. Therefore, an optimization is vital which would be geometry dependant.
- It was not possible to identify a thermal field able to produce simultaneously a large bonding area and a thin IMC layer for the optimization of the joint strength. Parallel weld seams could be an alternative solution to increase the bonding area without increasing the IMCs.

Acknowledgements

Dr. Supriyo Ganguly acknowledges the support by Engineering and Physical Sciences Research Council (EPSRC) through grant number EP/J017086/1. Sonia Meco is grateful to BAE Systems Naval Ships and EPSRC the Centre for Innovative Manufacturing in Laser-based Production Processes through grant number EP/K030884/1 for providing financial support to this project. The underlying data can be accessed through the Cranfield University data repository at https://dx.doi.org/10.17862/cranfield.rd.4893209.

References

Assuncao, E., 2012. Investigation of Conduction to Keyhole Mode Transition. Cranfield University.

Borrisutthekul, R., Yachi, T., Miyashita, Y., Mutoh, Y., 2007. Suppression of intermetallic reaction layer formation by controlling heat flow in dissimilar joining of steel and aluminum alloy. Mater. Sci. Eng. A 467, 108–113. http://dx.doi.org/10.1016/j.msea.2007.03.049.

Bouche, K., Barbier, F., Coulet, a, 1998. Intermetallic compound layer growth between solid iron and molten aluminium. Mater. Sci. Eng. A 249, 167–175. http://dx.doi.org/10.1016/S0921-5093(98)00573-5.

British Standard Instiurion, 2001. BS EN ISO 14273:2001 Specimen Dimensions and Procedure for Shear Testing Resistance Spot, Seam and Embossed Projection Welds. London.

Colegrove, P., Williams, S.W., Ikeagu, C., Thistlethwaite, A., 2009. The impact of different types of welding processes on the residual stress and distortion in 4 mm thick butt welds of ship plate. In: David, S.A., DebRoy, T., DuPont, J.N., Koseki, T., Smartt, H.B. (Eds.), Trends In Welding Research 2009: Proceedings of the 8th International Conference. ASM International Georgia, USA. pp. 758–765.

Cozzolino, L., 2013. Finite Element Analysis of Localised Rolling to Reduce Residual Stress and Distortion. Cranfield University.

Ding, J., Colegrove, P., Mehnen, J., Ganguly, S., Almeida, P.M.S., Wang, F., Williams, S., 2011. Thermo-mechanical analysis of wire and arc additive layer manufacturing process on large multi-layer parts. Comput. Mater. Sci. 50, 3315–3322. http://dx.doi.org/10.1016/j.commatsci.2011.06.023.

Fan, J., Thomy, C., Vollertsen, F., 2011. Effect of thermal cycle on the formation of intermetallic compounds in laser welding of aluminum-steel overlap joints. Phys. Proced. 12, 134–141. http://dx.doi.org/10.1016/j.phpro.2011.03.017.

Khandkar, M.Z.H., Khan, J.A., Reynolds, A.P., 2003. Prediction of temperature distribution and thermal history during friction stir welding: input torque based model. Sci. Technol. Weld. Join. 8, 165–174. http://dx.doi.org/10.1179/136217103225010943.

Kim, D., Badarinarayan, H., Kim, J.H., Kim, C., Okamoto, K., Wagoner, R.H., Chung, K., 2010. Numerical simulation of friction stir butt welding process for AA5083-H18 sheets. Eur. J. Mech. − A/Solids 29, 204–215. http://dx.doi.org/10.1016/j.euromechsol.2009.10.006.

Ltd., I.A, 2009. Tutorial to Get Started with the AxioVision Imaging System .

Ma, J., Harooni, M., Carlson, B., Kovacevic, R., 2014. Dissimilar joining of galvanized high-strength steel to aluminum alloy in a zero-gap lap joint configuration by two-pass laser welding. Mater. Des. 58, 390–401. http://dx.doi.org/10.1016/j.matdes.2014.01.046.

Mathieu, A., Shabadi, R., Deschamps, A., Suery, M., Matteı, S., Grevey, D., Cicala, E., 2007. Dissimilar material joining using laser (aluminum to steel using zinc-based filler wire). Opt. Laser Technol. 39, 652–661. http://dx.doi.org/10.1016/j.optlastec.2005.08.014.

Meco, S., Ganguly, S., Williams, S., McPherson, N., 2014. Effect of laser processing parameters on the formation of intermetallic compounds in Fe-Al dissimilar welding. J. Mater. Eng. Perform. 23, 3361–3370. http://dx.doi.org/10.1007/s11665-014-1106-5.

Ozaki, H., Kutsuna, M., 2009. Laser-roll welding of a dissimilar metal joint of low carbon steel to aluminium alloy using 2 kW fibre laser. Weld. Int. 23, 345–352. http://dx.doi.org/10.1080/09507110802542718.

Preston, R.V., 2000. Modelling of Residual Stresses in Welded Aerospace Alloys. University of Cambridge.

Quintino, L., Assuncao, E., 2013. Conduction laser welding. In: Katayama, S. (Ed.), Handbook of Laser Welding Technologies. Woodhead Publishing Limited, pp. 6–9. http://dx.doi.org/10.1533/9780857098771.1.139.

Schubert, E., Zerner, D.I., Sepold, P.G., 1997. Laser beam joining of material combinations for automotive applications. In: SPIE 3097, Lasers in Material Processing. Munich. pp. 212–221. http://dx.doi.org/10.1117/12.281079.

Shahverdi, H.R., Ghomashchi, M.R., Shabestari, S., Hejazi, J., 2002. Microstructural analysis of interfacial reaction between molten aluminium and solid iron. J. Mater. Process. Technol. 124, 345–352.

Shi, Q.Y., Dickerson, T., Shercliff, H.R., 2003a. Thermo-mechanical FE modelling of friction stir welding of A2024 including tool loads. In: 4th International Symposium on Friction Stir Welding. Park City, Utah, USA. p. 12.

Shi, Q.Y., Dickerson, T., Shercliff, H.R., 2003b. Thermo-mechanical analyses of welding aluminum alloy with TIG and friction stir welding. In: Trends in Welding Research 2002: Proceedings of the 6th International Conference ASM International. Pine Mountain, GA. pp. 247–252.

Simar, A., Pardoen, T., De Meester, B., 2006. Effect of boundary conditions and heat source distribution on temperature distribution in friction stir welding. Sci. Technol. Weld. Join. 11, 170–177. http://dx.doi.org/10.1179/174329306X84409.

Simar, A., Pardoen, T., De Meester, B., 2007. Effect of rotational material flow on temperature distribution in friction stir welds. Sci. Technol. Weld. Join. 12, 324–333. http://dx.doi.org/10.1179/174329307X197584.

Springer, H., Kostka, a., Payton, E.J., Raabe, D., Kaysser-Pyzalla, a., Eggeler, G., 2011. On the formation and growth of intermetallic phases during interdiffusion between low-carbon steel and aluminum alloys. Acta Mater. 59, 1586–1600. http://dx.doi.org/10.1016/j.actamat.2010.11.023.

Suder, W.J., Williams, S.W., 2012. Investigation of the effects of basic laser material interaction parameters in laser welding. J. Laser Appl. 24, 032009. http://dx.doi.org/10.2351/1.4728136.

Sun, Y., Zang, Y., ShiQ, Y., 2009. High precision modelling of welding and post welding cold rolling continuous processing numerical simulation. In: Proceedings of The Second International Conference on Modelling and Simulation. Manchester, England. pp. 312–318.

Wang, X., Wood, J.V., Sui, Y., Lu, H., 1998. Formation of intermetallic compound in iron-aluminum alloys. J. Shanghai Univ. (Engl. Ed.) 2, 305–310. http://dx.doi.org/10.1007/s11741-998-0045-5.

Wang, H., Colegrove, P.A., Santos, J., 2013. Hybrid modelling of 7449-T7 aluminium alloy friction stir welded joints. Sci. Technol. Weld. Join. 18, 147–153. http://dx.doi.org/10.1179/1362171812Y.0000000078.

Wang, H., 2011. Numerical and Artifitial Neural Network Modelling of Friction Stir Welding. Cranfield University.

Williams, S., Suder, W., 2011. Use of fundamental laser material interaction parameters in laser welding. In: Conference on Lasers and Electro-Optics (CLEO) 2011. IEEE Baltimore, MD. pp. 1–2.